DOI 10.1007/s10891-022-02653-1
Journal of Engineering Physics and Thermophysics, Vol. 95, No. 7, November, 2022

MICROSTRUCTURE AND MECHANICAL PROPERTIES OF A (TiB + TiB_2 + TiC)/Ti–6Al–4V COMPOSITE MATERIAL FORMED IN THE PROCESS OF *IN SITU* SYNTHESIS IN SELECTIVE LASER MELTING

A. A. Golyshev, A. G. Malikov, V. M. Fomin, A. A. Filippov, and A. M. Orishich†

UDC 669

A study has been made of the physicomechanical properties of a heterogeneous material based on TiB, TiB_2, TiC, and B_4C ceramics and a Ti–6Al–4V metal alloy formed by the method of selective laser melting. Consideration has been given to the influence of TiB, TiB_2, TiC, and B_4C ceramic particles produced by in situ synthesis in the process of laser action on the microstructure and hardness of the formed metal-matrix composite. Basic mechanisms of variation in the microstructure to form secondary ceramic inclusions were discussed and microhardness measurements at a macro- and nanolevel were carried out. It has been established that ceramic particles formed as a result of the in-situ synthesis improve sharply the hardness of the metal-matrix composite depending on the composition of the ceramics.

Keywords: *additive technologies, CO_2-laser, boron carbide, Ti–6Al–4V, microstructure, microhardness, nanohardness, in situ and ex situ synthesis.*

Introduction. The technology of selective laser melting (SLM) is considered to be one of the most advanced technologies of additive manufacturing and permits fabricating, with powder mixtures, intricately shaped parts with high precision [1–4]. The SLM has shown a good performance in growing metal-matrix composite materials with high service properties.

Composites reinforced by ceramic particles are advanced materials owing to their high specific modulus and strength, and also to the excellent stability to wear compared to metal alloys [5, 6]. Various ceramic materials (TiC, TiB, TiB_2, WC, Cr_3C_2, B_4C, and others) have been investigated to date as reinforcing particles for cermet composites [6–8]. However, boron carbide B_4C which is widely used to create abrasive materials, strong coatings, and lightweight armor is worth noting individually owing to its superior mechanical properties [9–11].

Metal-matrix composite materials can be obtained with different approaches. The first is the *ex situ* method, in which reinforcing particles are added directly to the metal melt pool. Another method is *in situ* synthesis in which reinforcing particles are formed in the composite resulting from the chemical reactions between the matrix and ceramics elements. The main advantage of the *in situ* synthesis technology compared to the *ex situ* one is the smaller difference between the coefficient of thermal expansion of the ceramic particles and the matrix, which leads to a reduction in the propagation of cracks [12].

At present, there are numerous works on investigating the additive growth of a Ti–B_4C system with a varying content of B_4C to create a (TiC + TiB + TiB_2)–Ti metal-matrix composite [13, 14]. It is well known that TiB, TiB_2, and TiC possess good compatibility with the titanium matrix in view of the similar coefficients of thermal expansion [1]. Furthermore, TiC increases the composite's hardness, and TiB improves creep resistance. As a result, the metal-matrix composite (TiC + TiB + TiB_2)–Ti exhibits a vast potential for meeting various industrial requirements.

In the present investigation, we have studied the influence of ceramic TiB, TiB_2, TiC, and B_4C particles produced by *in situ* synthesis in the process of laser exposure of a microstructure and the mechanical characteristics of the formed metal-matrix composite with TiB, TiB_2, and TiC inclusions. In the work, we discuss basic mechanisms of variation in the

†Deceased.

S. A. Khristianovich Institute of Theoretical and Applied Mechanics, Siberian Branch of the Russian Academy of Sciences, 4/1 Institutskaya Str., Novosibirsk, 630090, Russia; email: alexgol@itam.nsc.ru. Translated from Inzhenerno-Fizicheskii Zhurnal, Vol. 95, No. 7, pp. 1851–1858, November–December, 2022. Original article submitted November 30, 2021.

 0062-0125/22/9507-1802 ©2022 Springer Science+Business Media, LLC

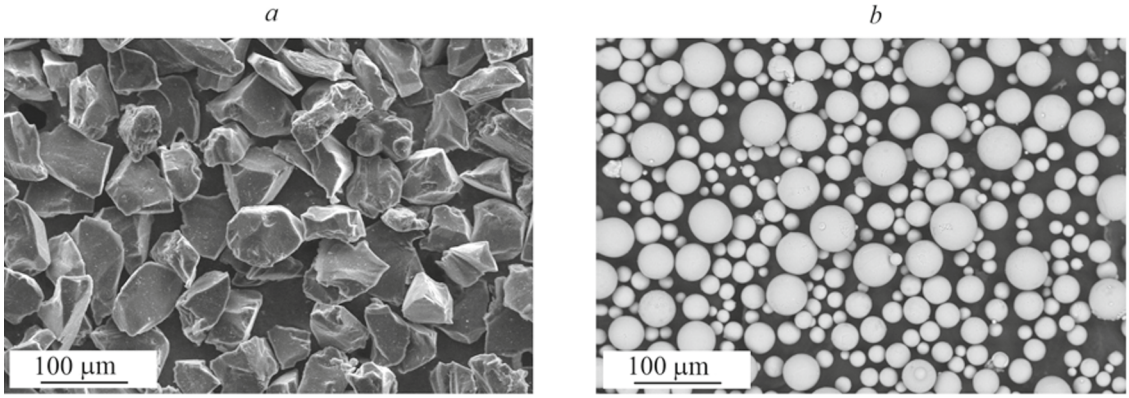

Fig. 1. Electron-microscope image of the used powders: a) B_4C and b) Ti–6Al–4V.

microstructure and phase composition to form secondary ceramic inclusions; measurements of microhardness at a micro and nanolevel have been carried out.

Methods and Equipment. A B_4C–Ti–6Al–4V powder mixture was prepared by mechanical mixing in a Venus FTLMV-02 V-shaped mixer with a varying ratio of the components during one hour until a homogeneous powder mixture was formed. The powder of boron carbide B_4C had the form of fragmental particles (Fig. 1a) with an average size of 40 μm. The powder of titanium alloy Ti–6Al–4V with spherically shaped particles of 10 to 45 μm was used as the metallic matrix (Fig. 1b). By the method of selective laser melting (SLM), the powder mixture was clad onto the substrate in the form of a plate from titanium alloy Ti–6.5Al–1.8Zr–1.5Mo with dimensions 50 × 50 × 5 mm.

The automated laser technological complex (ALTC) "Sibir'" on the basis of a gas-discharge continuous CO_2 laser was used as the source of laser radiation. This complex has been developed at the S. A. Khristianovich Institute of Theoretical and Applied Mechanics of the Siberian Branch of the Russian Academy of Sciences [15].

To determine the phase composition, we carried out synchrotron-radiation (SR)-assisted investigation on a unit of the Mega Science class at the G. I. Budker Institute of Nuclear Physics of the Siberian Branch of the Russian Academy of Sciences at the station "Diffractometry in Hard X Rays". The use of synchrotron radiation permits determining the phase composition in a material's 3D volume.

The microstructure of clad layers was investigated with an Olympus LEXT OLS 3000 optical confocal microscope and using a Zeiss EVO 15 scanning electron microscope equipped with two detectors: a detector of backward-scattered electrons and a detector of secondary electrons. Microhardness measurements were carried out with a Wilson Hardness Group Tukon 1102 meter, and nanohardness measurements, with a NanoScan spectrometer.

A specimen with dimensions 4 × 4 mm and a thickness of 1 mm was investigated throughout the height using SR with a wavelength of 0.3685 Å in the Debye–Scherrer geometry. The shooting was carried out successively, beginning with the top layer, in the range from 0 to 22° with a step of 100 μm. The beam diameter was 100 μm.

Experimental Results and Discussion. When a multilayer cermet composite is created first it is necessary to seek the optimum parameters of exposure of a powder mixture to laser radiation in forming single tracks. We varied such parameters, as the laser-radiation power W, the scanning velocity V, the focal position f, and the powder-layer thickness t. As a result of optimization, we found the following parameters: W = 1000 W, V = 16.6 mm/s, f = 16 mm below the surface of the powder layer, and t = 0.3 mm.

Figure 2 gives the cross-sectional structure of the clad B_4C–Ti–6Al–4V mass with a 1:9% mass ratio, obtained with the scanning electron microscope. From the distribution of B_4C-ceramics particles in Fig. 2, we can observe a periodic layered structure which forms the clad mass.

Chemical reactions play a key role in growing a metal-matrix composite. To understand the principles of this process, it is necessary to study the thermodynamic properties of a reactive system. We write possible reactions in the system B_4C–Ti–6Al–4V [16]

$$\mathrm{TiC + C = TiC}\ , \tag{1}$$

$$\mathrm{Ti + 3Al = TiAl_3}\ , \tag{2}$$

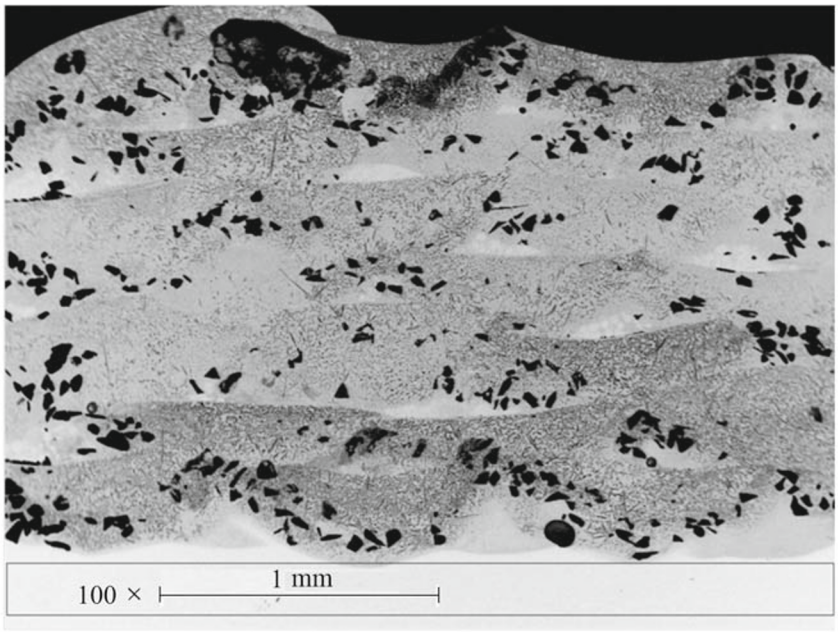

Fig. 2. SEM image of the cross section of the B_4C–Ti–6Al–4V specimen with a mass ratio of 1:9%.

TABLE 1. Calculated Values of the Changes in the Enthalpy, the Entropy, and the Gibbs Free Energy

Reactions	ΔH (J·mole^{-1})	ΔS (J·mole^{-1}·K^{-1})	ΔG (J·mole^{-1})
(1)	–184 096	–12.134	–184 096 + 12.314T
(2)	–142.256	–21.032	–142 256 + 21.032T
(3)	–62 342	–8.568	–62 342 + 8.568T
(4)	−256 898	−8.540	–256 898 + 8.540T
(5)	−260 246	–18.874	–260 246 + 18.874T
(6)	–753.538	–17.114	–753 538 + 17.114T
(7)	−760 234	–37.782	–760 234 + 37.782T

$$2Al + B_4C = 2AlB_2 + C\,, \tag{3}$$

$$Ti + AlB_2 = TiB_2 + Al\,, \tag{4}$$

$$2TiB + AlB_2 = 2TiB_2 + Al\,, \tag{5}$$

$$5Ti + B_4C = 4TiB + TiC\,, \tag{6}$$

$$3Ti + B_4C = 2TiB_2 + TiC\,. \tag{7}$$

In the B_4C–Ti–6Al–4V system, the probability and priority of the chemical reactions are associated with the Gibbs energy (ΔG) of each reaction. From the available thermodynamic data [16], we can calculate changes in the Gibbs free energy in reactions (1)–(7). The change in the Gibbs free energy is determined by the expression

$$\Delta G = \Delta H - T\Delta S\,, \tag{8}$$

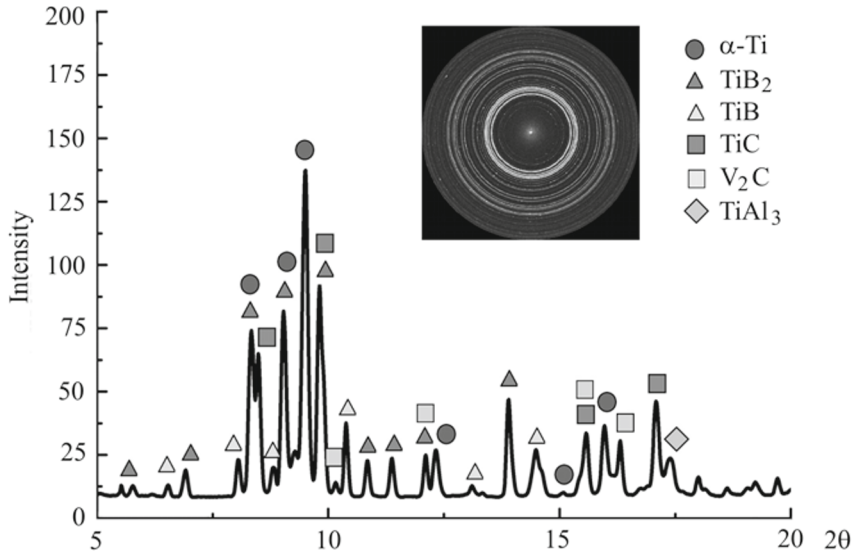

Fig. 3. Results of the analysis of SR rings of the cross section of the B_4C–Ti–6Al–4V specimen with a ratio of 1:9 wt.%.

where ΔH, ΔS, and T are the standard enthalpy and entropy changes and the thermodynamic temperature respectively. Table 1 gives the enthalpy and entropy changes and the Gibbs free energy in reactions (5)–(11) [16].

In the temperature interval 1100–2000 K, all the values of the Gibbs free energy of chemical reactions (1)–(7) are negative suggesting the chemical reaction proceeding in this temperature interval. It can be seen from Table 1 that the Gibbs free energy of reactions (6) and (7) is much lower than in reactions (1)–(5). This points to the higher priority of reactions (6) and (7). The value of the Gibbs free energy of formation of TiB_2 is lower (7) than in TiB. This speaks of the priority of TiB_2 for the formation of TiB in the reaction. Thus, the reaction of TiB_2 formation is thermodynamically easier than the reaction of TiB formation. However, noteworthy is one important fact: although TiB_2 is easier to generate thermodynamically than TiB, the coefficient of diffusion of the boron from TiB_2 into the titanium matrix and the rate of growth of TiB are very high; this leads to the fact that it is TiB, not TiB_2, that must be the actual product [6].

Figure 3 gives the diffraction patterns in SR-produced transmitted light. As a result, the presence of the great amount of phase compounds in the clad layer is shown. It can be seen from Fig. 3 that the specimen with a Ti–6Al–4V–B_4C cladding with a 9:1% ratio includes α-Ti, TiB_2, TiB, TiC, V_2C, and $TiAl_3$. No B_4C ceramics has been found. It may be assumed that the exposure of the B_4C–Ti–6Al–4V mixture to laser radiation in optimum regimes gave rise to *in situ* synthesis to form a cermet composite based on α-Ti and reinforcing TiB_2, TiB, TiC, V_2C, and $TiAl_3$ particles.

A detailed microstructure of a typical individual layer of mass, which has been obtained with high-resolution scanning microscopy, is presented in Fig. 4a. It can be seen that inside each layer, we can single out several different zones. Zone 1 is of complex morphology and represents a great number of different structures (Fig, 4b). From the energy-dispersive analysis and the literature data, it may stated that the darkest needle structures (wiskers) represent a boron-titanium compound (TiB) and the second structure are submicron grains arranged around the entire periphery of the wiskers. After the elemental analysis, it has been obtained that these grains represent titanium carbide TiC.

Zone 2 (Fig. 4c) represents a set of small grains with characteristic dimensions of 2–3 μm. According to the results obtained by the method of energy-dispersive x-ray spectroscopy (EDX) with SR (Fig. 3) and on the basis of the literature data, it may be established that the dark grain in Fig. 4c represents the compound of boron and titanium (TiB_2), and the light grain, titanium carbide (TiC).

Figure 5 gives the photographs of indentations in different zones. It can be seen that in elongated wiskers and in small grains, the values of microhardness are similar and are 1292 and 1253 HV0.3 respectively. However, it should be noted that the indentation is several times larger than the structures under study. As a result, the value of microhardness shows the averaged value of the set of different grains.

To understand the influence of the content of secondary phase particles (TiB, TiB_2, and TiC) on the hardness of the formed metal-matrix composite B_4C–Ti–6Al–4V manufactured by the SLM method, the specimen's hardness is measured

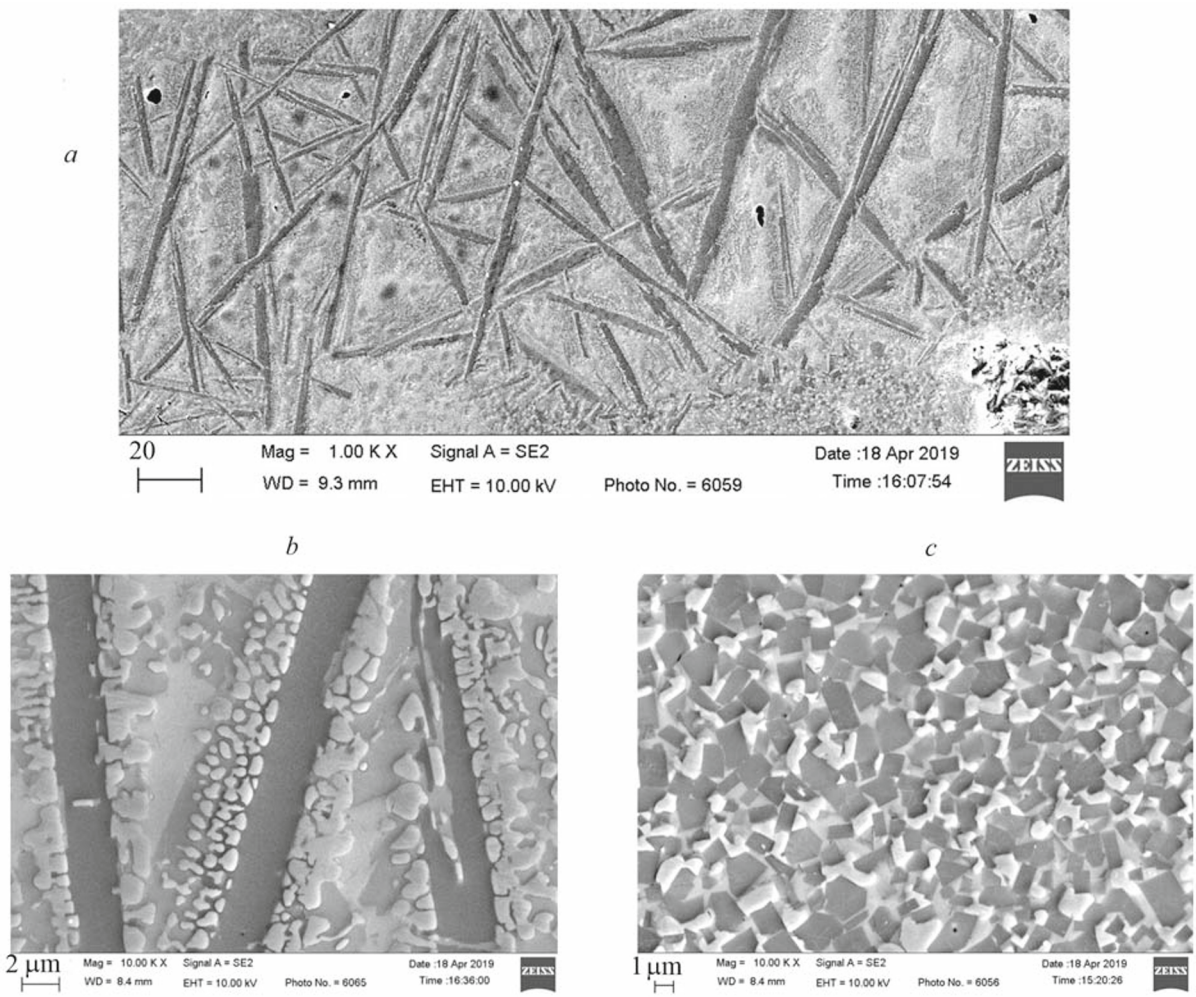

Fig. 4. SEM image of the microstructure of the $B_4C–BT_6$ specimen with a mass ratio of 1:9%: a) individual layer; b) zone 1; c) zone 2.

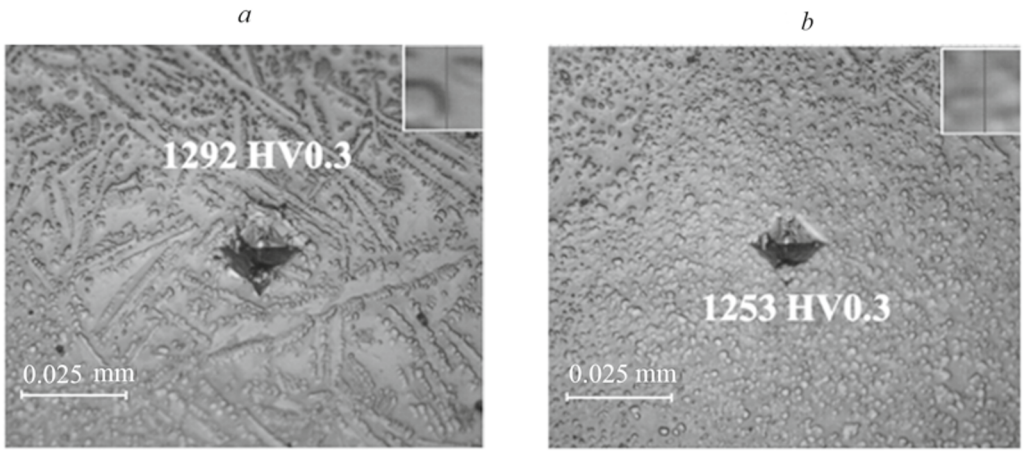

Fig. 5. Images of the $B_4C–BT_6$ specimen with a mass ratio of 1:9% with the impressions from the microindenter on different portions.

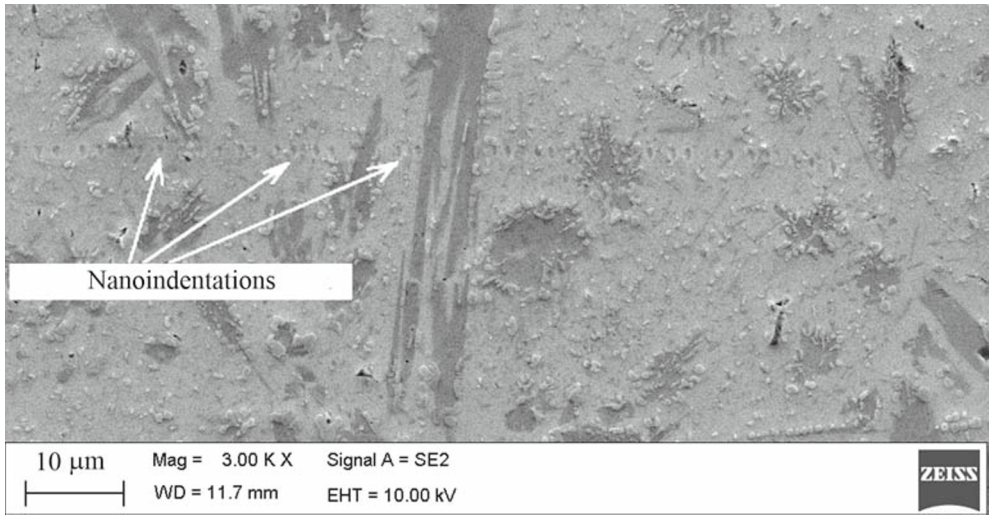

Fig. 6. Images of the B_4C–BT_6 specimen with a mass ratio of 1:9% with the impression from the nanoindenter.

using nanoindentation tests. Figure 6 shows the image from the electron microscope with the impressions as a result of nanoindentation (50 pricks). It has been obtained that the average hardness of the metal matrix is approximately 7.5 GPa. However, in the case where indentation of secondary reinforcing particles (wiskers) was carried out the hardness grew to 24 GPa.

Conclusions. The run of experiments on investigating the laser cladding of a B_4C–Ti–6Al–4V cermet powder mixture was conducted. The phase composition of a metal-matrix composite resulting from the laser exposure of the B_4C–Ti–6Al–4V mixture was established with SR for the first time. It has been noted that as a result of the laser exposure in optimum regimes, *in situ* synthesis occurred to form a cermet composite based on α-Ti and reinforcing TiB_2, TiB, TiC, V_2C, and $TiAl_3$ particles which were absent from the original powder mixture.

Measurements of the micro- and nanohardness of the metal-matrix composite were carried out. In nanoindentation, it has been obtained that the average hardness of the metal matrix is approximately 7.5 GPa, and of the secondary reinforcing particles, 24 GPa.

Acknowledgments. This work was carried out owing to grant No. 21-19-00733 of the Russian Science Foundation. The investigation on nanoindentation was conducted with the equipment of the Collective Use Center "Mekhanika" (S. A. Khristianovich Institute of Theoretical and Applied Mechanics of the Siberian Branch of the Russian Academy of Sciences).

NOTATION

f, focal position, mm; *T*, thermodynamic temperature, K; *t*, powder-layer thickness, μm; *V*, scanning velocity, m/min; *W*, laser-radiation power, W; ΔH, standard enthalpy change, $J \cdot mole^{-1}$; ΔS, standard entropy change, $J \cdot mole^{-1} \cdot K^{-1}$.

REFERENCES

1. Z. Chen, L. Ziyong, L. Junjie, et al., 3D printing of ceramics: A review, *J. Eur. Ceram. Soc*., **39**, No. 4, 661–687 (2019).
2. Ch. Cai, R. Chrupcala, Z. Jinliang, et al., *In situ* preparation and formation of TiB/Ti–6Al–4V nanocomposite via laser additive manufacturing: Microstructure evolution and tribological behavior, *Powder Technol*., **342**, 73–84 (2019).
3. V. M. Fomin, A. A. Golyshev, A. G. Malikov, et al., Creation of a functionally gradient material by the selective laser melting method, *J. Appl. Mech. Tech. Phys*., **61**, No. 5, 878–887 (2020).
4. Yu. P. Sharkeev, A. I. Dmitriev, A. G. Knyazeva, et al., Selective laser melting of the Ti–(40–50) wt.% Nb alloy, *High Temp. Mater. Proc.*, **21**, 161–183.5 (2017)
5. S. Ford and D. Mélanie, Additive manufacturing and sustainability: An exploratory study of the advantages and challenges, *J. Clean. Prod.*, **137**, 1573–1587 (2016).

6. L. Le, T. Minasyan, R. Ivanov, et al., Selective laser melting of TiB_2–Ti composite with high content of ceramic phase, *Ceram. Int.*, **46**, No. 13, 21128–21135 (2020).
7. D. Ngo Tuan, Al. Kashani, G. Imbalzano, et al., Additive manufacturing (3D printing): A review of materials, methods, applications and challenges, *Composites. Part B: Eng.*, **143**, 172–196 (2018).
8. G. Munro Ronald, Material properties of titanium diboride, *J. Res. Nat. Inst. Standards Technol*., **105**, No. 5, 709–720 (2000).
9. V. M. Fomin, A. A. Golyshev, V. F. Kosarev, et al., Deposition of cermet coatings on the basis of Ti, Ni, WC, and B_4C by cold gas dynamic spraying with subsequent laser irradiation, *Phys. Mesomech.*, **23**, No. 4, 291–300 (2020).
10. B. Basu, G. B. Raju, and A. K. Suri, Processing and properties of monolithic TiB_2 based materials, *Int. Mater. Rev.*, **51**, No. 6, 352–374 (2006).
11. A. A. Golyshev, A. M. Orishich, and A. A. Filippov, Formation of B_4C–Ti–6Al–4V cermet coatings by the method of SLM, *Metal Sci. Heat Treatment*., **62**, Nos. 11–12, 696–700 (2021).
12. Wu Xiaolei, *In situ* formation by laser cladding of a TiC composite coating with a gradient distribution, *Surf. Coat. Technol.*, **115**, Nos. 2–3, 111–115 (1999).
13. A. Golyshev and A. Orishich, Microstructure and mechanical characterization of Ti–6Al–4V–B_4C metal ceramic alloy, produced by laser powder-bed fusion additive manufacturing, *Int. J. Adv. Manuf. Technol.*, **109**, Nos. 1–2, 579–588 (2020).
14. Anal Animesh, T. K. Bandyopadhyay, and K. Das, Synthesis and characterization of TiB_2-reinforced iron-based composites, *J. Mater. Proc. Technol.*, **172**, No. 1, 70–76 (2006).
15. A. A. Golyshev, A. M. Orishich, and A. A. Filippov, Similarity laws in laser cladding of cermet coatings, *J. Appl. Mech. Tech. Phys.*, **60**, No. 4, 758–767 (2019).
16. Yi Junchao, Xiaowei Zhang, Rao Jeremy Heng, et al., *In-situ* chemical reaction mechanism and non-equilibrium microstructural evolution of (TiB_2 + TiC)/AlSi10Mg composites prepared by SLM-CS processing, *J. Alloys Comp*., **857**, Article ID 157553 (2021).